Materials Science & Engineering A 677 (2016) 58–67

Contents lists available at ScienceDirect

Materials Science & Engineering A

journal homepage: www.elsevier.com/locate/msea

Cyclic deformation and fatigue of rolled AZ80 magnesium alloy along different material orientations

Ying Xiong [a,b,*], Yanyao Jiang [c]

[a] Key Laboratory of Special Purpose Equipment and Advanced Processing Technology, Ministry of Education, Zhejiang University of Technology, Hangzhou, Zhejiang 310032, China
[b] College of Mechanical Engineering, Zhejiang University of Technology, Hangzhou, Zhejiang 310032, China
[c] University of Nevada, Reno, Department of Mechanical Engineering, Reno, NV 89557, USA

ARTICLE INFO

Article history:
Received 8 July 2016
Received in revised form
8 September 2016
Accepted 9 September 2016
Available online 10 September 2016

Keywords:
Magnesium alloy
Cyclic deformation
Twinning
Material orientation
Fatigue life

ABSTRACT

The effect of material orientation on cyclic deformation and fatigue behavior of rolled AZ80 magnesium (Mg) alloy was experimentally investigated under fully reversed strain-controlled loading in ambient. The testing specimens were taken from a rolled AZ80 Mg plate at four orientations with respect to rolled plane: 0°(ND, normal direction), 30°(ND30), 60°(ND60), and 90°(RD, rolled direction). Fatigue fracture morphologies of specimens along different orientation were analyzed by scanning electron microscopy (SEM). Overall cyclic hardening was observed for the material loaded in different directions. For a given strain amplitude, the ND specimens had the lowest fatigue resistance among the specimens of all material orientations. The fatigue life of an ND30 specimens is similar to that of an ND60 specimen at a given strain amplitude and both are higher than that of an RD specimen when the strain amplitude is higher than 0.4%, whereas an RD specimen exhibits a better fatigue resistance when the strain amplitude is lower than 0.4%. A mixed fracture mode with transgranular and intergranular cracking related to lamellar-like features occurred during stable crack growth, and an intergranular fracture mode related to dimple-like features exhibited in the fast fracture region. A multiaxial fatigue model based on the strain energy density can correlate all the fatigue experiments of the material at different material orientations.

1. Introduction

In recent years, lightweight magnesium (Mg) alloys have been applied in transport and aerospace industries to improve energy efficiency. Wrought Mg alloys (rolled and extruded) are most promising for structural applications since they have excellent mechanical properties and fatigue resistance as compared to cast Mg alloys. In particular, wrought Mg-Al-Zn alloys are suitable for structural components because these alloys contain a small amount of manganese (Mn), which improves the corrosion resistance and the mechanical properties of the materials [1]. Structural components are usually subjected to cyclic loading, and fatigue may occur in service. Therefore, it is necessary to systemically investigate the cyclic deformation behavior and fatigue properties of Mg alloys for the design and evaluation of the Mg structures.

It is well known that wrought Mg alloys with a hexagonal close-packed (hcp) crystal structure have strong textures formed by the rolling and extrusion processes. The texture leads to a significant anisotropy due to the activation of different deformation modes such as slips and $\{10\bar{1}2\}$ tension twinning [2]. This implies that the fatigue behavior of wrought Mg alloys can be significantly influenced by the loading direction with respect to the material orientation.

Studies were conducted the fatigue behavior of wrought Mg-Al-Zn alloys including extruded AZ31 [3,4], extruded AZ61 [1,5], and rolled AZ31 or AZ31B [6–15]. Limited fatigue experiments were conducted using the rolled Mg alloys whose loading axial directions were oriented parallel to the transverse direction (TD), rolled direction (RD), and normal direction (ND). Wu et al. [6] investigated the strain-controlled low-cycle fatigue behavior of rolled AZ31B Mg alloy with RD, TD and ND orientations. It was found that the ND sample had the worst fatigue life among the three orientation samples, and the fatigue properties of the RD sample was similar to that of the TD sample. In contract, Park et al. [7–9] pointed out that the low cycle fatigue (LCF) life of an ND sample was longer than that of an RD sample. It was also reported the effect of the initial $\{10\bar{1}2\}$ twins on the fatigue deformation

* Corresponding author at: College of Mechanical Engineering, Zhejiang University of Technology, Hangzhou, Zhejiang 310032, China.
E-mail addresses: yxiong@zjut.edu.cn (Y. Xiong), yjiang@unr.edu (Y. Jiang).

http://dx.doi.org/10.1016/j.msea.2016.09.031
0921-5093/

behavior of rolled AZ31 Mg alloy by pre-compressive on the ND samples. Lv et al. [12,13] compared the fatigue properties of a rolled AZ31 alloy along different orientations under both the stress-controlled and strain-controlled cyclic loading, and found that the fatigue lives of the TD samples were longer than these of the RD samples. Zhang et al. [15] reported the effects of sample orientation on the ratcheting behavior of a hot-rolled AZ31B Mg alloy. These studies indicate that the initial orientation of the testing specimen with respect to the rolled direction plays an important role on the mechanical properties and fatigue resistance of wrought Mg alloys. However, previous work entirely concentrates on typical three material orientations (TD, RD and ND). The effect of other orientations on fatigue behavior has not been well understood. On the other hand, the rolled sheet were usually used to study the influence of material orientation on mechanical properties [2,11–13,15]. The problem is that the loading path of different orientation specimens is on the same RD-TD plane, namely, loading direction is perpendicular to the *c*-axes of the crystallographical lattice. This results in the deformation mechanism of these specimens being similar due to the fact that $\{10\bar{1}2\}$ tension twinning can occur when a tensile load is applied perpendicular to the RD-TD plane. The sheets do not allow for the study of the material orientation influence because of the limited thickness that does not allow for the testing in the thickness direction. For application of the wrought Mg alloys to load-bearing components, it is important to evaluate fatigue properties along different orientations or loading paths.

In the present study, the effect of material orientation on the cyclic deformation and fatigue behavior was investigated with specimens taken from a rolled AZ80 Mg alloy thick plate with four different orientations with respect to the rolled plane: 0° (ND), 30° (ND30), 60° (ND60), and 90° (RD). Monotonic mechanical properties, cyclic stress-strain response, fractography characteristics, and fatigue life were experimentally investigated. An energy based fatigue model was evaluated for its capability to predict the fatigue life of the anisotropic Mg alloy.

2. Materials and experimental

2.1. Materials and specimens

The Mg alloy used in the study is a hot-rolled AZ80 Mg plate (Mg-7.8% Al-0.36% Zn-0.04%Mn, in wt%) with a thickness of 60 mm. The material was homogenized at 340 °C for 2.5 h. Fig. 1 shows the original microstructure of the material. The three-dimensional stereography was obtained using an optical microscope (OM). The microstructure and the pole figures observed by electron back scattered diffraction (EBSD) on the ND–TD plane are shown in Fig. 1b and c, respectively. The microstructure was characterized by equiaxed grain α-matrix and β-$Mg_{17}Al_{12}$ phases distributing along the grain boundaries. The average gain size was approximately 50 μm measured by the linear intercept method. The {0002} pole figure exhibits an intense basal texture with *c*-axes aligned parallel to the ND. There was no preferred orientation for the $\{10\bar{1}0\}$ prismatic plane or the $\{10\bar{1}1\}$ pyramidal plane, indicating that the *a*-axes were randomly oriented on the RD–TD rolled plane.

To investigate the effect of material orientation on cyclic deformation and fatigue behavior, specimens were machined from the rolled plate with the loading axes of the testing specimens along 0° (ND), 30° (ND30), 60° (ND60) and 90° (RD) with respect to the rolled direction as shown in Fig. 2. The dog-bone shaped plate specimens for monotonic tensile and fatigue tests have a gage section of 8 mm × 4 mm × 4 mm. In order to avoid bulking, cylindrical specimens with a diameter of 10 mm and gage length of 15 mm were used for monotonic compression tests. Before testing, the surface of the gage section of the specimen was polished by using silicon carbide papers with grit No. from 400 up to 1200.

2.2. Experiments

All the monotonic and strain-controlled cyclic loading

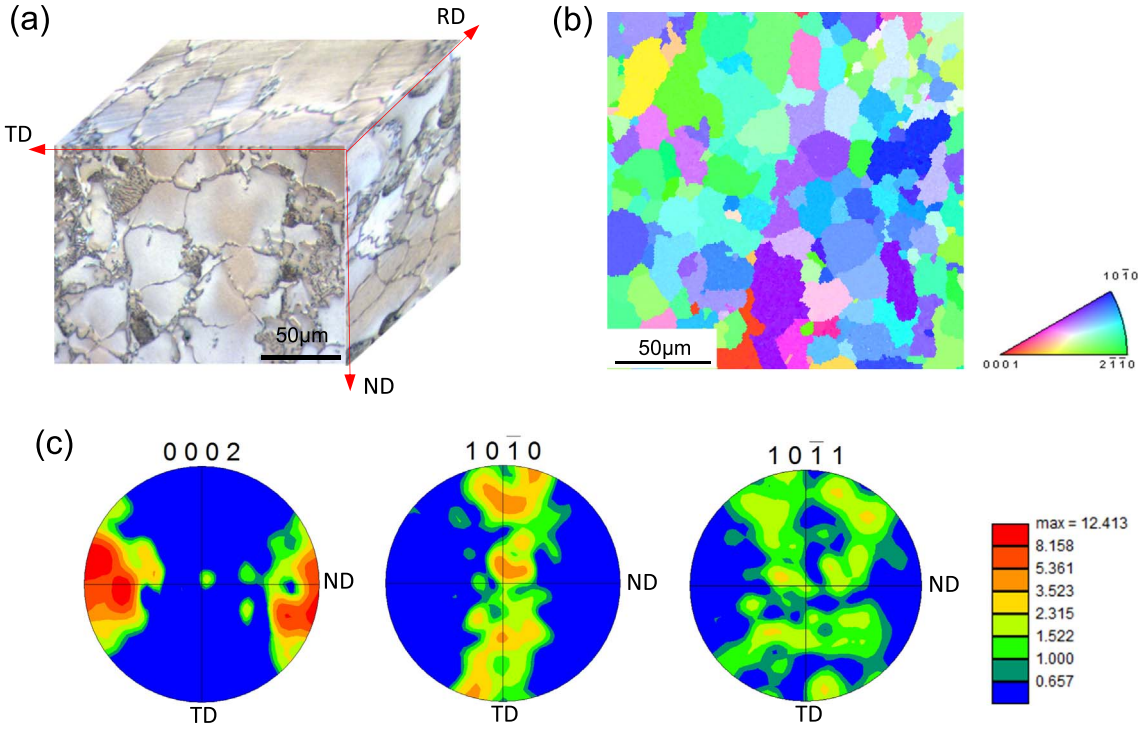

Fig. 1. Initial microstructure and texture of rolled AZ80 Mg alloy: (a) three-dimensional optical image; (b) microstructure obtained by EBSD; and (c) (0002) $\{10\bar{1}0\}$ and $\{10\bar{1}1\}$ pole figures measured by EBSD.

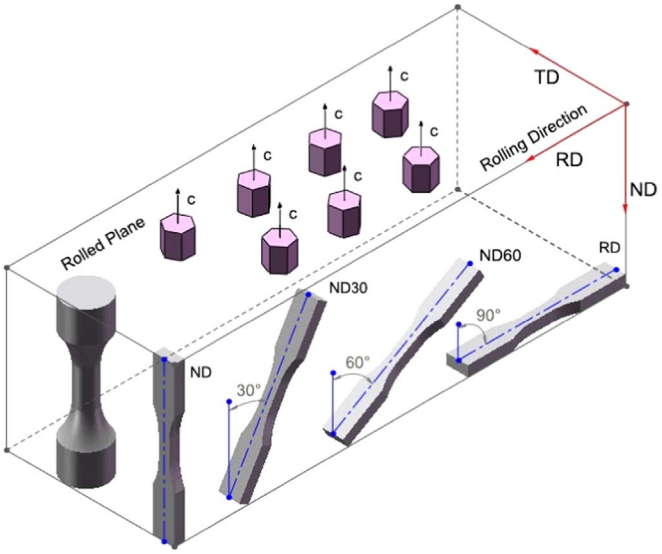

Fig. 2. Illustration of different orientation specimens and approximate texture.

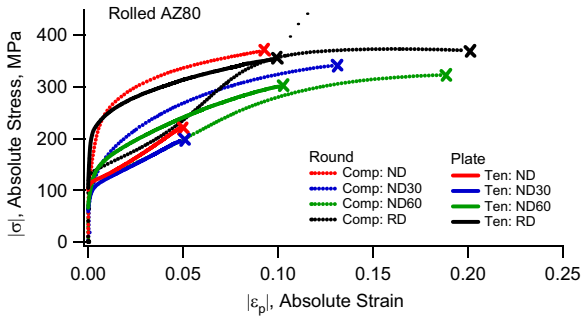

Fig. 3. Stress-plastic strain curves of rolled AZ80 Mg alloy under monotonic tension and monotonic compression for four orientation specimens.

Table 1
Static mechanical properties for different material orientations.

Mechanical properties	ND	ND30	ND60	RD
Elasticity Modulus (GPa)	46.9	44.5	43.3	44.3
0.2% offset yield stress in tension (MPa)	116	98	114	203
0.2% offset yield stress in compression (MPa)	155	100	98	134
True fracture stress under tension (MPa)	220	195	299	352
True fracture stress under compression (MPa)	366	339	321	372
Elongation under tension (%)	4.9	4.8	10.1	9.8
Elongation under compression (%)	9.0	13.0	18.7	20.5
Reduction in area (%) under tension	5.1	5.1	10.9	10.7

experiments were conducted with an Instron testing machine at room temperature. The monotonic tension and monotonic compression experiments were conducted at a strain rate of 2×10^{-3}/s to determine the static mechanical properties of the material. The fatigue testing with a sine wave form and strain ratio of $R_\varepsilon=-1(R_\varepsilon=\varepsilon_{min}/\varepsilon_{max},)$ where ε_{min} is the minimum strain and ε_{max} is the maximum strain in a loading cycle) was applied at an approximate strain rate of 1×10^{-2}/s. The strain amplitude ranged from 0.002 to 0.02 and the corresponding testing frequencies ranged from 10 Hz to 0.2 Hz. All the fatigue experiments started with tension first followed by compression. The load and engineering strain outputs were recorded automatically by the computer data acquisition system. For each loading cycle, a minimum of 200 data points were recorded. Each fatigue specimen was tested until the specimen was completely fractured into two pieces, and the fatigue life was determined corresponding to the moment when the stress amplitude in a loading cycle displayed a 5% reduction from the maximum peak value.

3. Results and discussion

3.1. Tensile and compressive properties

The monotonic stress-plastic strain curves for different orientation specimens are shown in Fig. 3 and the mechanical properties are listed in Table 1. The reported stresses are the true stresses considering the change of the cross section of the testing specimens during deformation. The strains are logarithmic strains. It is found that the stress-plastic strain curves are strongly dependent on the material orientation. The strong tension-compression asymmetry displayed in the RD specimen is typical in the wrought Mg alloys [2]. The tensile flow curve shows a concave-down shape with a higher yield stress than that under compression. The compressive flow curve reveals a sigmoidal shape with tension twinning dominated concave-up curve followed by a slip dominated concave-down shape [2,6–9,12,13]. Comparing with the curve of the RD specimen, the stress-strain curves in the other three orientation specimens exhibit several characteristics. First, the elongations are dependent on the loading direction relative to the material orientation. The elongation of specimens in both tension and compression increases with the direction angle from 0° (ND) to 90° (RD). Under tension, the elongations of the ND (4.9%) and ND30 (4.8%) specimens are similar and are lower than these of the rest two material orientations. The elongation of the ND60 (10.1%) is similar to that of the RD (9.8%) specimen. Under compression, the RD specimen (19.8%) exhibits a highest elongation among all of the orientations, whereas the elongation of the ND specimen is approximately 9.0% which is lower than that of the ND30 (13.0%) and ND60 (18.7%) specimens. For a given material orientation, the elongation in compression is higher than that in tension.

The yield stress is not related to the material orientation if the tension twinning is the dominating plastic deformation mechanism, but it is dependent on the orientation if the plastic deformation is dominated by slips. As shown in Fig. 1 and Table 1, the stress-strain curves under tension in ND30 (98 MPa), ND60 (114 MPa) and RD (205 MPa) specimens have a concave-down shape, and the yield stress in tension increases with the increasing direction angle from 30° (ND30) to 90°(RD). On the other hand, the compressive stress-strain curves in ND (155 MPa), ND30 (100 MPa) and ND60 (98 MPa) specimens display a concave-down shape, and the yield stress under compression decreases with increasing direction angle from 0° (ND) to 60°(ND60). Usually, the yield stress with respect to the material orientation is attributed to different deformation modes, which is determined by the combined effect of Schmid Factor (SF) and Critical Resolved Shear Stress (CRSS) [16,17]. Similar results were reported in hot-rolled AZ61 [18] and rolled AZ31 [19].

3.2. Cycle stress-strain response

Fig. 4 shows the stress-strain hysteresis loops at half-fatigue lives at different total strain amplitudes for the specimens tested at four material orientations. It is noticed that the shape of the stress-strain hysteresis loops is dependent on the magnitude of strain amplitude and the initial material orientation. When the strain amplitude is higher than 0.4% for the RD specimens and 0.35% for the other three specimens (ND, ND30 and ND60), the tension-compression asymmetry becomes significant. For a given material orientation, the degree of asymmetry becomes more

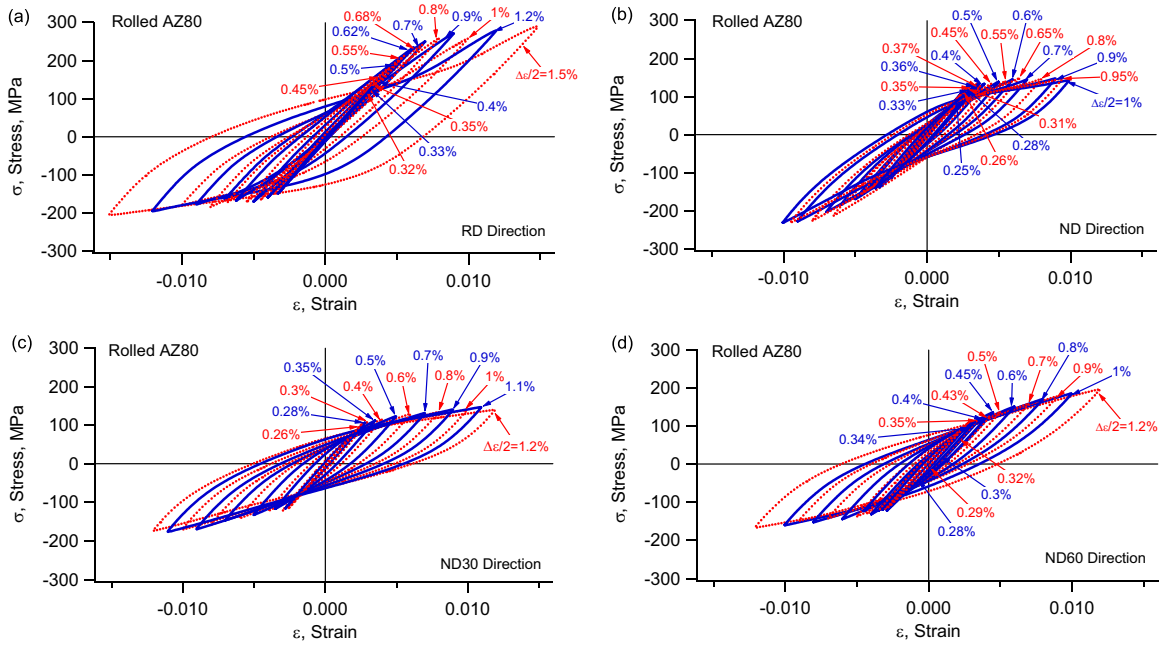

Fig. 4. Stress-strain hysteresis loops at half- fatigue lives for specimens of four orientations: (a) RD, (b) ND, (c) ND30, (d) ND60.

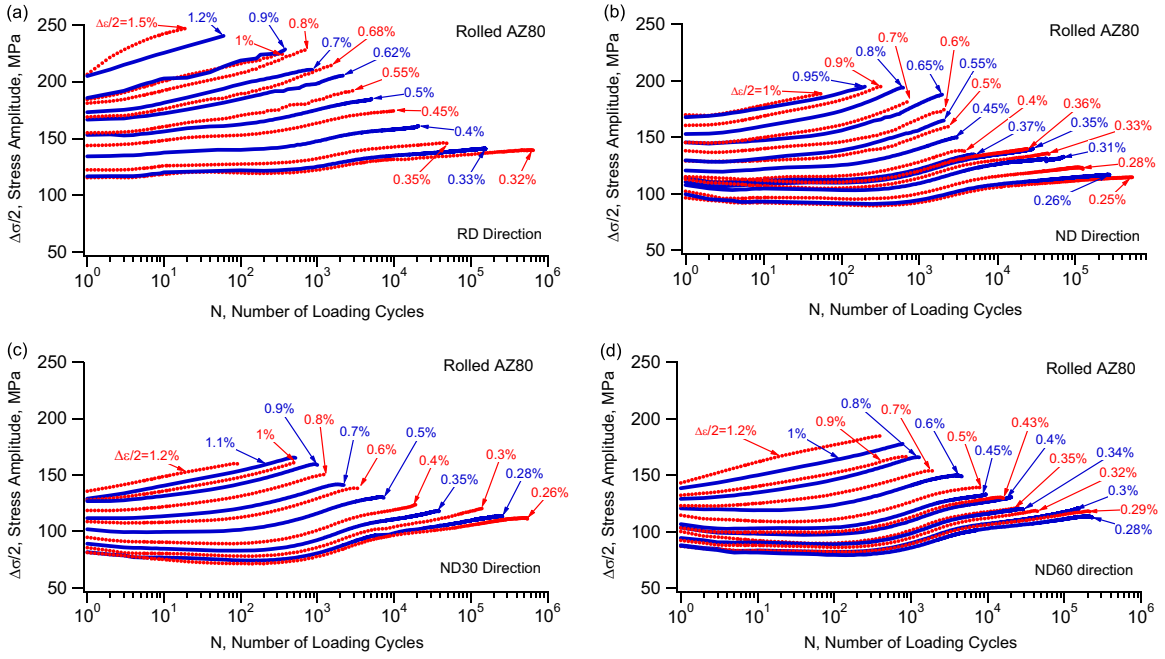

Fig. 5. Stress amplitude versus the number of loading cycles at various total strain amplitudes for four material orientations: (a) RD, (b) ND, (c) ND30 and (d) ND60.

severe with a higher strain amplitude. Dependent on the material orientation, a sigmoidal shape of the stress-strain curve can be in the tensile reversal or in the compressive reversal. For the RD specimens, the concave-up shape is observed in the compression reversal and a sigmoidal shape in the tension reversal. In contrast, the concave-up shape in the ND specimens shows in the tensile reversal and the compressive reversal exhibits a sigmoidal shape. However, for the other two orientation specimens, a slight sigmoidal shape is presented in the compressive reversal for the ND30 specimens or the tensile reversal for the ND60 specimens. When the strain amplitude is lower than 0.4% for the RD specimens and 0.35% for the other three specimens, the stress-strain hysteresis loops are symmetrical in shape.

Fig. 5 shows the evolution of stress amplitudes with the number of loading cycles at various total strain amplitudes for the four material orientations. For the RD specimens (Fig. 5a), the stress amplitudes evidently increase with the total strain amplitudes from 0.4% to 1.5%, displaying continued cyclic hardening behavior. When the strain amplitude is lower than 0.4%, the stress amplitude is almost constant for the first 1000 loading cycles, and slight cyclic hardening occurs thereafter. For the other three specimens (ND, ND30 and ND60), similar cyclic stress responses are observed as shown in Fig. 5b–d.

The evolution of stress-plastic strain hysteresis loops at a typical strain amplitude of 1% is analyzed for the effect of material orientation on the cyclic plastic deformation behavior. The plastic

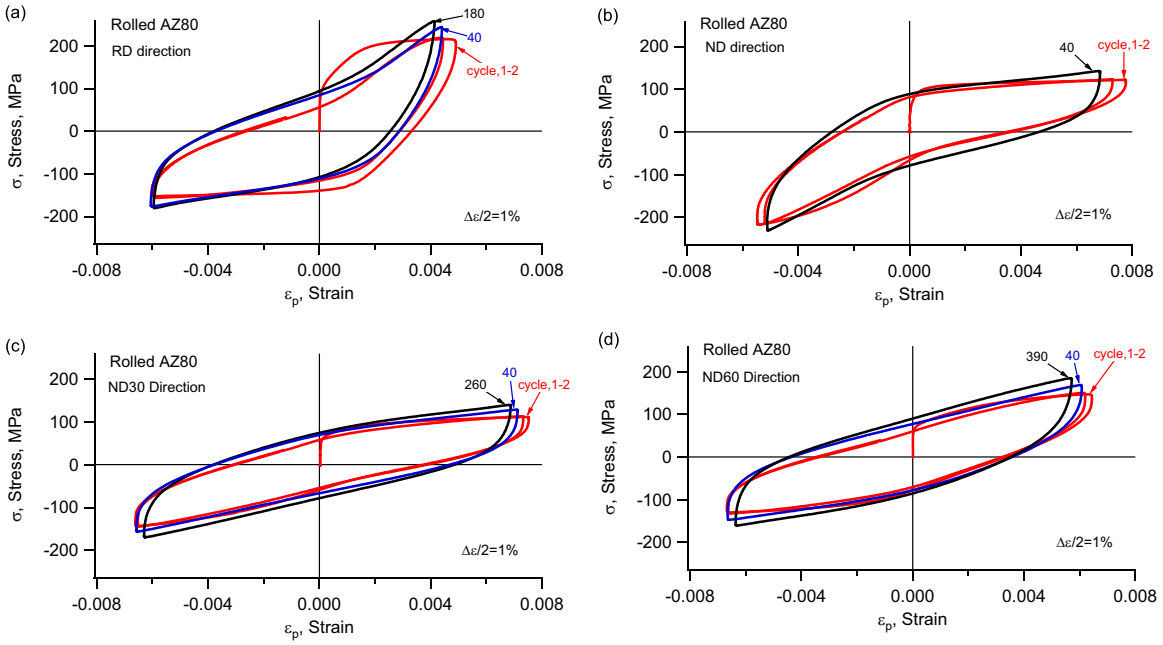

Fig. 6. Evolution of stress-plastic strain hysteresis loop at strain amplitude of 1% for four orientation specimens: (a) RD, (b) ND, (c) ND30, and (d) ND60.

strain is obtained by subtracting the elastic strain from the total strain,

$$\varepsilon_p = \varepsilon - \frac{\sigma}{E} \tag{1}$$

where ε, ε_p, E, and σ are the total strain, plastic strain, elasticity modulus, and stress, respectively.

Fig. 6 shows the evolution of stress-plastic strain hysteresis loops at a strain amplitude of 1% for the four material orientations. Primary $\{10\bar{1}2\}$ tension twinning occurs under tension parallel to the *c*-axes or compression perpendicular to the *c*-axes of grains [2]. At a strain amplitude of 1%, when the RD specimen (Fig. 6a) is loaded up to 1/4 cycle, the deformation behavior is identical to that under monotonic tension. Subsequent loading into the compression stage with the stress exceeding the yield stress (134 MPa) results in the activation of the $\{10\bar{1}2\}$ tension twinning. Although the fraction of twinned regions increases with the increasing plastic strain, the twinning capacity is not exhausted before the end of the compression reversal. As a result, a concave-up shape shows in the compressive reversal [6,17,20,21]. During subsequent tension reloading, the *c*-axis of the twinned lattice reorients approximately perpendicular to the rolled direction, which is associated with the detwinning process [20–26]. Detwinning diminishes progressively before the flowing stress reaches the maximum tensile stress, which is followed by non-basal slips operated as a primary mode for a further imposed strain. The process results in a sigmoidal shape in the tensile reversal. The inflection point in the sigmoidal shape curve corresponding to the exhaustion of detwinning becomes closer to the maximum tensile stress with increasing number of loading cycles. This indicates that the residual twins remain in tension loading owing to the delayed detwinning exhaustion, and the fraction of residual twins increases with the number of cycles [6,17]. It is noticed that starting from the second loading cycle, both the tensile and compressive peak stresses increase with the increase in loading cycles. Cyclic hardening in both tension and compression reversal is mainly due to the accumulated residual twin boundaries, as well as the increased dislocation densities [17,21–24]. In contrast, in the ND specimen (Fig. 6b), the *c*-axis of the original hexagonal cell is approximately parallel to the tensile loading direction, which leads to $\{10\bar{1}2\}$ tension twinning formed in first tensile reversal and detwinning in subsequent compression reversal.

The yield stress of the ND specimen under tension is less than that of the RD specimen. The material under investigation exhibits a basal texture at its initial state with random orientations of the *a*-axes on the RD-TD plane. This suggests that for the ND specimen, twinning can be easily activated during tension loading and the detwinning can be completed before the end of the compression reversal under fully reversed loading. Comparing Fig. 6a with Fig. 6b, it can be seen that the concave-down detwinning portion in the sigmoidal shape curve becomes longer for the RD specimen due to the delayed exhaustion of detwinning at higher strain levels. It can be speculated that the volume fraction of the residual twins in the RD specimen is higher than that in the ND specimen with increasing number of cycles, which is associated with a higher activity of hard non-basal slips occurring in further plastic deformation after detwinning is exhausted. This explains why the stress amplitudes of the RD specimens is higher than that of the ND specimens at a given strain amplitude (refer to Fig. 5). In addition, with the increase in the volume fraction of the residual twins in the RD specimen, plastic deformation becomes more difficult to occur due to the interaction between the accumulated residual twin boundaries and the increased dislocation slips. The process results in a lower plastic strain amplitude than that of the ND specimen at the same number of loading cycles.

When the specimen orientation is between 0° and 90°, as shown in Fig. 6c and d, the degree of asymmetry of the stress-strain hysteresis loops is reduced comparing to either the RD or ND specimen. Since the *c*-axes of a few lattices may be approximately parallel to the loading direction, deformation twinning may occur during early tensile reversal for the ND30 specimen or compressive reversal for the ND60 specimen. As can be seen from Fig. 6c and d, the sigmoidal shaped curves present in both tension and compression reversals even when the loading cycles reach a half of the fatigue life. It is noticed that the twins form during the tension reversal for the ND30 specimen or compression reversal for the ND60 specimen and complete before the stress reaches the peak stress. The detwinning process completes before the stress reaches the maximum compressive stress (ND30) or the maximum tensile stress (ND60) during each loading cycle. This

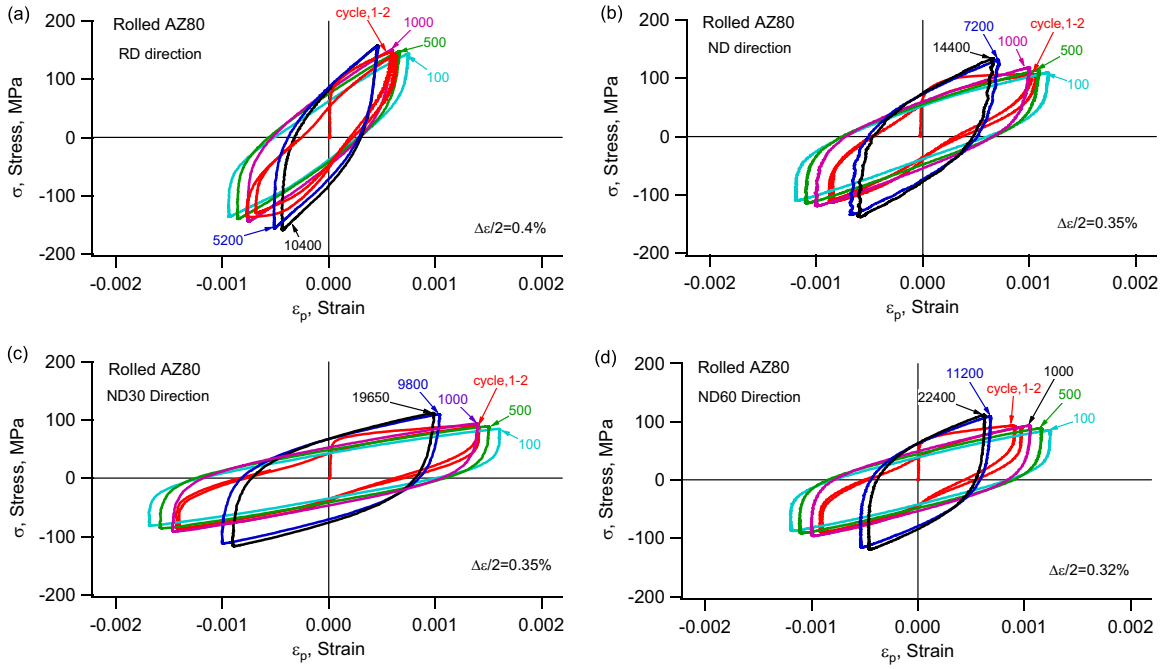

Fig. 7. Evolution of stress-plastic strain hysteresis loop at lower strain amplitudes for four orientation specimens: (a) RD, 0.4% (b) ND, 0.35% (c) ND30, 0.35% and (d) ND60, 0.32%.

requires the activation of the slip systems to accommodate the further strain after twinning or detwinning is exhausted. Because the volume fraction of twins are considerably low in the ND30 and ND60 specimens, the capacities of the residual twins and the non-basal slips are lower as compared to these of the RD and ND specimens. This causes a marginal increase in the flow stress after twinning or detwinning is exhausted. Therefore, the peak stresses measured in both the tension and compression reversals for the ND60 and ND 30 specimens are significantly lower than these of the RD and ND specimens at a given strain amplitude (Fig. 5).

Fig. 7 shows the evolutions of the stress-plastic hysteresis loops at lower strain amplitudes for the four orientation specimens. The 1st, 2nd, 100th, 500th, 1000th, a quarter-lives, and half-lives cycles (black solid line) are plotted for each loading case. When the strain amplitude is 0.4% for the RD specimen (Fig. 7a), the maximum tensile stress (approximately 146 MPa) during early cyclic loading is lower than the monotonic tensile yield stress (205 MPa) and is not sufficient to activate macroscopic yielding. In contrast, the maximum compression stress (approximately 136 MPa) slightly exceeds the monotonic compressive yield stress (134 MPa), which indicates that few tension twins can be formed in the compression reversal, causing plastic strain that is increased with the number of cycles before 100 cycles. However, the sigmoidal shape of the stress-strain hysteresis loop is not obvious due to the exhaustion of new tension twinning and the absence of twinning and detwinning activities [20]. After 100 loading cycles, slip becomes a primary deformation mode. The strain hardening rate gradually increases with increasing number of loading cycles, and the range of plastic strain decreases as the stress-plastic strain hysteresis loops becomes narrower and tend to become symmetric after 1000 cycles.

Similar evolution behavior is observed in other three specimens at a similar strain amplitude, but the shapes of the stress-strain hysteresis loops are different from that of the RD specimen. As an example with ND30 specimen (Fig. 7c), the stress-strain hysteresis loops with a slight sigmoidal shape exhibit in both the tension and compression reversals until fatigue failure. It can be seen from Fig. 7c that the tensile peak stress (~94 MPa) and the compressive peak stress (~ 95 MPa) in the first loading cycle is close to the monotonic tension yield stress (98 MPa) and the compressive yield stress (100 MPa), respectively. This suggests that a few $\{10\bar{1}2\}$ tension twins favorable for crystallographic reorientation of 86.3° can be formed during early cyclic loading. Because tension twinning is activated during the first few loading cycles, the basal planes originally unfavorably oriented for twinning may be reoriented to more favorable orientations in twined regions, leading to the observed cyclic softening in the early loading stage before 500 cycles. With increasing number of cycles, the volume fraction of twins and basal slips increase. As a result, the plastic strain amplitude at a given strain amplitude for the ND30 specimen is higher than that in the ND specimen at the same number of loading cycles (Fig. 7b and c).

3.3. *Fatigue fracture morphologies*

Fig. 8 shows SEM images of the fractured surfaces at a total strain amplitude of 0.4% for the four material orientations. Fig. 8a, d, g and j presents overall views of the fracture surfaces of the tested specimens. The fracture surface can be divided into three regions: crack nucleation site (red dotted line and marked with A), stable crack propagation region (white dotted line and marked with B), unstable crack propagation, and the final rapid fracture region (and marked with C). For all the tested specimens, crack initiation is observed to occur on the specimen surface. Multiple crack initiation locations are observed on the surface of the ND specimen.

High-magnified images taken in the region B near the crack nucleation site are shown in Fig. 8b, e, h and k. The fatigue crack propagation regions are characterized by transgranular cracking with a cleavage feature. This region of all the orientation specimens also exhibits flake-like feature, which is more randomly oriented with each other in conjunction with some micro-cracks. Such a feature at the lower strain amplitude might be resulted from the twinning–detwinning process together with the repeated blunting-sharpening process due to dislocation slips in the plastic zone at the fatigue crack tip [27]. Additionally, the particles are the

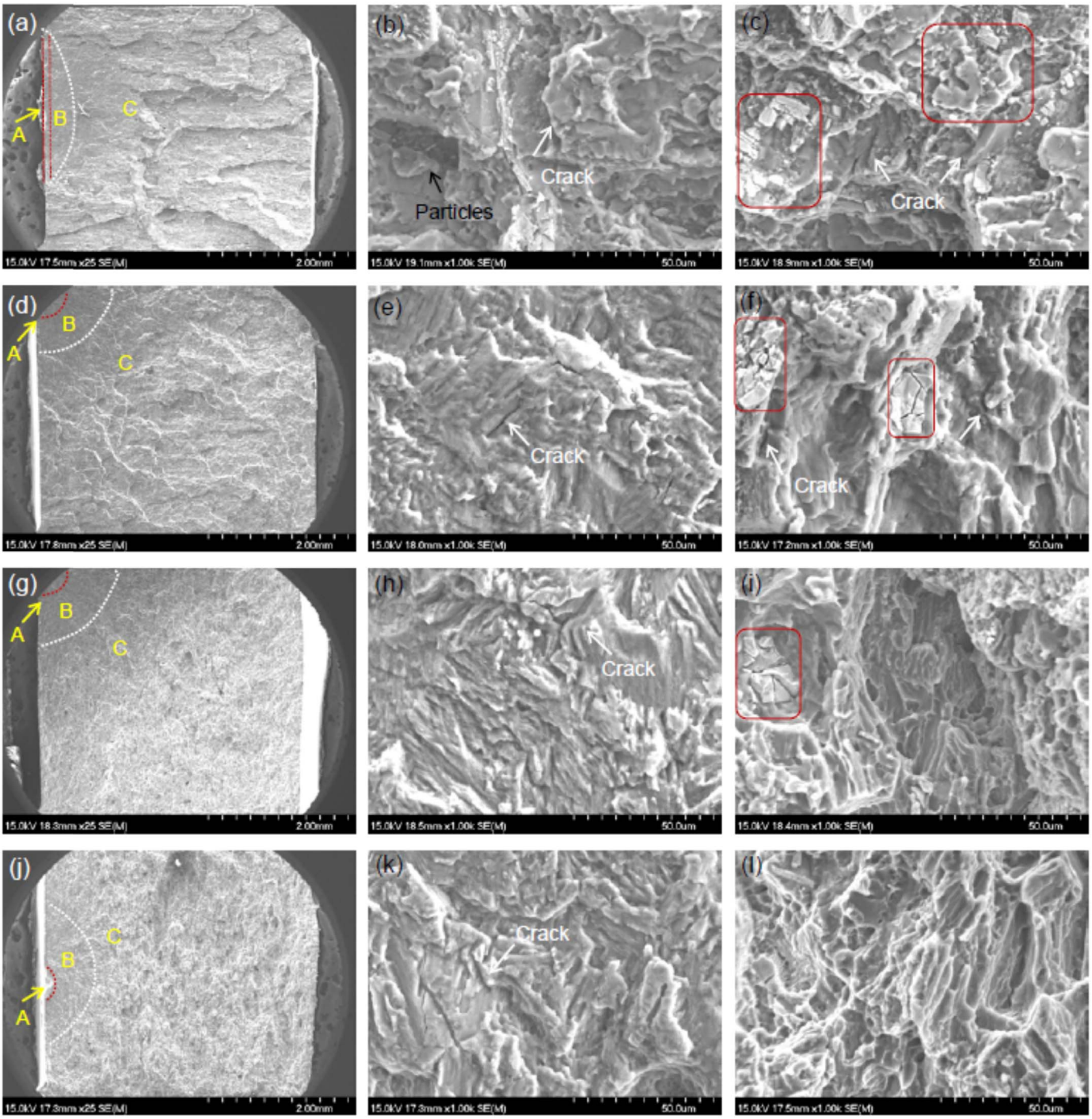

Fig. 8. SEM images of fractured surface at a strain amplitude of 0.4% for four orientation specimens: (a)–(c) ND, (d)–(f) ND30, (g)–(i) ND60 and (j)–(l) RD.

possible sources of crack initiation in the ND specimens, as shown in Fig. 8b. Because the rolled Mg alloy is heated directly at high temperature in air before the rolling process and Mg alloys are more readily oxidized due to their intense chemical activity with oxygen [28–30], oxides and the intermetallic particles are easily formed on the interior rolled texture plane. For the ND specimen (Fig. 8b), the loading axis is perpendicular to the rolled texture plane and as a result, micro-cracks could be incubated and generated in the interface between the inclusion and the matrix with a tensile stress.

High-magnified images taken in region C are shown in Fig. 8c, f, i and l. It is noticed that a quasi-cleavage facets with some secondary crack exhibit in the ND and ND30 specimens. In addition, fracturing of the intermetallic particles is observed in Fig. 8c, f and i (as indicated by red solid line box), respectively, which could be caused by pressured stress due to the contact between the two crack planes during compression loading. On the other hand, the dimple-like features in this fast fracture region become more evident as the orientation angle increasing from 30° (ND30) to 90° (RD), which is an intergranular fracture mode similar to the fracture surface of tensile specimen. In this case, $Mg_{17}Al_{12}$ particles deposited on the grain boundaries may contribute to the final crack growth.

3.4. Fatigue life

All the fatigue test results for the four orientation specimens are shown in Tables 2–5. The axial strain amplitude, stabilized stress amplitude, axial mean stress and plastic strain energy density values are taken from the stress–strain hysteresis loop at the half-fatigue lives for a given specimen.

The fatigue lives as a function of the total strain amplitude are presented in Fig. 9. As can be seen from Fig. 9, the fatigue life of an ND specimen is lowest among all orientations at a given strain amplitude. The fatigue lives of the ND30 specimens are similar to those of the ND60 specimens, and both are higher than the RD specimens at strain amplitudes over 0.4%. When the strain amplitude is lower than 0.4%, the fatigue life of the RD specimen is longest. As discussed in the previous sections, material exhibits different cyclic deformation behavior dependent on the strain amplitude. At higher strain amplitudes, twining-detwinning dominates the cyclic plastic deformation throughout the whole fatigue life for all the four orientation specimens. At lower strain amplitudes, dislocation slips dominate the cyclic plastic deformation in the RD specimens, and transition from twinning-detwinning to dislocation slips occurs in ND, ND30 and ND60 specimens during cyclic loading.

Table 2
Strain-controlled fatigue experiments for ND specimen.

Spec ID	$\Delta\varepsilon/2$ (%)	f (Hz)	σ_m (MPa)	$\Delta\sigma/2$ (MPa)	N_f	ΔW_p (MJ/m^3)
80PN003	1	0.333	−44.0	184.6	67	1.638
80PN0029	0.95	0.4	−41.7	189.1	206	1.532
80PN0021	0.9	0.4	−39.6	187.2	330	1.390
80PN0025	0.8	0.6	−39.8	185.9	620	1.093
80PN0022	0.7	0.75	−28.9	173.6	760	0.833
80PN0020	0.65	0.8	−31.2	179.5	1960	0.725
80PN0017	0.6	0.8	−19.9	167.2	2140	0.614
80PN0018	0.55	0.9	−17.8	158.3	2072	0.511
80PN006	0.5	1	−15.1	153.6	2380	0.429
80PN0026	0.45	1.25	−10.3	144.0	3020	0.346
80PN0011	0.4	1.5	−1.5	134.2	3760	0.272
80PN0028	0.37	2	−3.3	130.5	5200	0.219
80PN0036	0.36	1.75	−3.4	136.6	24580	0.179
80PN008	0.35	2	−0.9	135.8	28760	0.163
80PN0033	0.33	2	−4.8	132.6	46000	0.119
80PN0035	0.31	2.5	0.4	130.2	71016	0.086
80PN0014	0.28	3	0.0	121.2	> 125950	0.052
80PN0027	0.26	4	1.5	115.1	> 274006	0.020
80PN0019	0.25	4/8	−0.9	113.6	543150	0.006

$\Delta\varepsilon/2$: axial strain amplitude, $\Delta\varepsilon/2 = (\varepsilon_{max} - \varepsilon_{min})/2$ where ε_{min} is the minimum strain and ε_{max} is the maximum strain in a loading cycle; f: frequency; σ_m: axial mean stress, $\sigma_m = (\sigma_{max} + \sigma_{min})/2$; $\Delta\sigma/2$: axial stress amplitude, $\Delta\sigma/2 = (\sigma_{max} - \sigma_{min})/2$; N_f: number of loading cycles to failure; ΔW_p: plastic strain energy density per loading cycle.

Table 3
Strain-controlled fatigue experiments for ND30 specimen.

Spec ID	$\Delta\varepsilon/2$ (%)	f (Hz)	σ_m (MPa)	$\Delta\sigma/2$ (MPa)	N_f	ΔW_p (MJ/m^3)
80PNR305	1.2	0.25	−17.0	156.2	101	2.263
80PNR3014	1.1	0.3	−14.8	160.8	520	2.088
80PNR303	1	0.333	−15.0	155.1	536	1.730
80PNR3017	0.9	0.4	−14.4	154.8	1013	1.445
80PNR306	0.8	0.45	−11.8	145.8	1280	1.159
80PNR308	0.7	0.75	−7.5	138.6	2239	0.919
80PNR3010	0.6	0.8	−5.9	134.8	3573	0.740
80PNR3012	0.5	1	−4.7	127.4	7340	0.542
80PNR309	0.4	1.5	−3.3	118.8	18880	0.335
80PNR3013	0.35	2/3	−2.3	114.1	38600	0.235
80PNR3011	0.3	2/4	−6.2	115.4	140600	0.104
80PNR3015	0.28	2/5	−4.6	111.1	258800	0.054
80PNR3016	0.26	2/6/10	−6.4	110.4	> 560826	0.020

Table 4
Strain-controlled fatigue experiments for ND60 specimen.

Spec ID	$\Delta\varepsilon/2$ (%)	f (Hz)	σ_m (MPa)	$\Delta\sigma/2$ (MPa)	N_f	ΔW_p (MJ/m^3)
80PNR6021	1.2	0.25	14.4	180.9	439	2.571
80PNR6022	1	0.333	11.7	172.5	782	1.798
80PNR6014	0.9	0.4	14.3	163.1	920	1.444
80PNR608	0.8	0.6	8.8	161.4	1320	1.153
80PNR6011	0.7	0.7	7.8	150.1	1980	0.896
80PNR607	0.6	0.75	3.3	147.6	4620	0.701
80PNR605	0.5	1	−0.6	136.8	8300	0.485
80PNR609	0.45	1.3	6.2	129.5	9580	0.386
80PNR6018	0.43	1.5	−2.6	128.0	16140	0.345
80PNR606	0.4	1.5	−5.2	126.5	20400	0.283
80PNR6012	0.35	2.5	−4.8	117.5	25250	0.198
80PNR6015	0.34	2.5	−2.7	117.3	29200	0.187
80PNR6016	0.32	2.5	−4.0	115.3	44800	0.142
80PNR6013	0.3	2.5	−2.5	115.6	> 153360	0.075
80PNR6020	0.29	4	−6.4	115.6	> 218800	0.051
80PNR6023	0.28	2/6	−1.4	111.5	> 230600	0.043

Table 5
Strain-controlled fatigue experiments for RD specimen.

Spec ID	$\Delta\varepsilon/2$ (%)	f (Hz)	σ_m (MPa)	$\Delta\sigma/2$ (MPa)	N_f	ΔW_p (MJ/m^3)
80PR0024	1.5	0.2	41.5	244.4	33	4.428
80PR0054	1.2	0.25	41.5	236.6	78	2.729
80PR0013	1	0.333	38.6	218.8	366	1.687
80PR0043	0.9	0.4	47.1	224.3	395	1.305
80PR0044	0.8	0.45	42.8	221.7	756	0.985
80PR0023	0.7	0.75	43.1	207.0	878	0.640
80PR0062	0.68	0.7	34.9	206.2	1520	0.593
80PR0061	0.62	0.75	33.6	201.4	2160	0.441
80PR0052	0.55	0.9	20.6	191.2	2940	0.347
80PR0021	0.5	1.5	10.9	181.2	5100	0.270
80PR0051	0.45	1.25	7.1	172.4	10260	0.183
80PR0031	0.4	2	−1.0	158.0	20800	0.124
80PR0032	0.35	4	−4.2	144.7	> 50200	0.072
80PR0042	0.33	3/5/8	−9.4	129.7	156140	0.034
80PR0063	0.32	2/10	−8.4	139.0	650602	0.009

The plastic strain energy density per loading cycle is obtained by integrating the area of the stress-plastic strain hysteresis loop,

$$\Delta W_p = \oint_{cycle} \sigma d\varepsilon^p \tag{2}$$

where σ is the stress and ε^p is the plastic strain as being defined by Eq. (1). A fatigue model with the plastic strain energy density can be expressed as follows [31]:

$$\Delta W_p N_f^m = C \tag{3}$$

where ΔW_p and N_f are the plastic strain energy density per loading cycle and fatigue life, respectively. m and C are material constants. Fig. 10 shows the relationship between ΔW_p and fatigue life for all the specimens tested. The results are presented in log–log scales. The solid straight line is an approximate medium line of the ΔW_p-N_f curve of all the specimens tested, and the two dotted lines are the factor-of-three boundaries. Obviously, almost all the test data points are within the factor-of-three lines. The results show that the ΔW_p parameter correlates well the fatigue experiments of the rolled AZ80 alloy for different material orientations. The ΔW_p parameter was reported to be suitable for the prediction of low-cycle fatigue life of the rolled AZ31 Mg alloy [32].

Fig. 11 shows the relationship between the mean stress and the

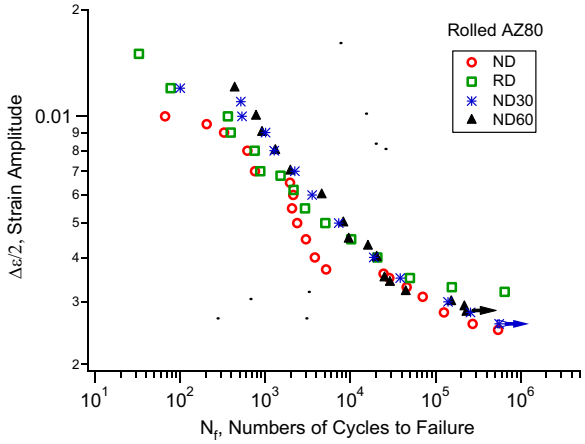

Fig. 9. Strain-life curves for four orientation specimens.

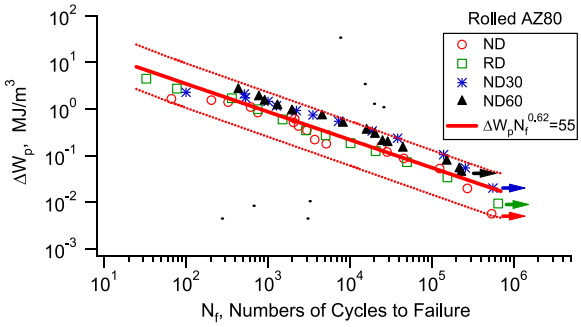

Fig. 10. Plastic strain energy density versus fatigue lives for four orientation specimens.

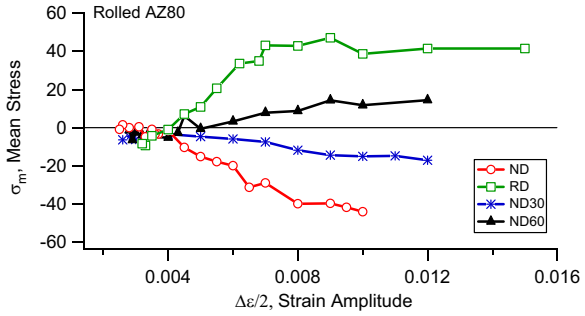

Fig. 11. Relationships of the mean stress and the strain amplitude for four orientation specimens.

strain amplitude for the specimens of four material orientations. At a strain amplitude below 0.4%, the mean stress is practically zero, which is approximately corresponding to a symmetric stress-strain hysteresis loop as shown in Fig. 4. When the strain amplitude is higher than 0.4%, compressive mean stresses are found in both the ND and ND30 specimens and the values increase with increasing strain amplitude. In contrary, tensile mean stresses are presented in the ND60 and RD specimens, and the values increase with the strain amplitude when the strain amplitude ranges from 0.4% to 0.9%. The mean stress is almost constant when the strain amplitude is larger than 0.9%. It is noticed that an energy fatigue model such as that represented by Eq. (3) does not consider the mean stress effect on fatigue.

4. Conclusions

Fully reversed strain-controlled fatigue experiments of a rolled AZ80 magnesium alloy were conducted in ambient to investigate the effect of the material orientation on the cyclic deformation and fatigue behavior. Testing specimens were fabricated with four orientations with respect to rolled plane: 0°(ND, normal direction), 30°(ND30), 60°(ND60), and 90°(RD, rolled direction). Major conclusions are summarized as follows.

(1) At higher strain amplitudes, the stress-strain hysteresis loops exhibit a strong asymmetry in the RD and ND specimens but a weak asymmetry in the ND30 and ND60 specimens. At lower strain amplitudes, the stress-strain hysteresis loops are symmetrical in shape for the specimens tested with material taken from different material orientations.
(2) Overall cyclic hardening is observed for the material tested at different material orientations and strain amplitudes. At a strain amplitude below 0.35%, slight and short-lived cyclic softening is observed at the start of the cyclic experiments in the ND30 and ND60 specimens.
(3) Twinning–detwinning dominates cyclic plastic deformation at higher strain amplitudes for the specimens of all material orientations, whereas dislocation slips dominate cyclic plastic deformation at lower strain amplitudes. A transition from twinning–detwinning to dislocation slips is observed during cyclic deformation in the ND30 and ND60 specimens when the strain amplitude is approximate 0.35%.
(4) At a given strain amplitude, the ND specimen has the lowest fatigue resistance among the four orientation specimens. The fatigue life of the ND30 specimen is similar to that of the ND60 specimen and both are higher than that of the RD specimen at a strain amplitude over 0.4%. The fatigue life of the RD specimen is the longest at a strain amplitude below 0.4%.
(5) Fatigue crack initiates from the surface of specimen. Transgranular cracking related to lamellar-like features occurs during stable crack growth, and an intergranular fracture mode related to dimple-like features exhibits in fast fracture region.
(6) The mean stresses are minimal when the strain amplitude is lower than 0.4%. When the strain amplitude is larger than 0.4%, compressive mean stresses are observed in the ND and ND30 specimens, and tensile mean stresses exist in the ND60 and RD specimens.
(7) A fatigue model based on the plastic strain energy density per

loading cycle is found to be suitable for predicting the fatigue life of the rolled Mg alloy with different material orientations.

Acknowledgements

The author gratefully acknowledges financial supports provided by the National Natural Science Foundation of China (No. 51275472), and the Natural Science Foundation of Zhejiang Province (No. LY12E05024). Yanyao Jiang thanks support from the National Science Foundation (CMMI-1462885).

References

[1] Z.B. Sajuri, Y. Miyashita, Y. Hosokai, Y. Mutoh, Effects of Mn content and texture on fatigue properties of as-cast and extruded AZ61 magnesium alloys, Int. J. Mech. Sci. 48 (2006) 198–209.
[2] X.Y. Lou, M. Li, R.K. Boger, S.R. Agnew, R.H. Wagoner, Hardening evolution of AZ31B Mg sheet, Int. J. Plast. 23 (2007) 44–86.
[3] F. Lv, F. Yang, S.X. Li, Z.F. Zhang, Effects of hysteresis energy and mean stress on low-cycle fatigue behaviors of an extruded magnesium alloy, Scr. Mater. 65 (2011) 53–56.
[4] Y.J. Wu, R. Zhu, J.T. Wang, W.Q. Ji, Role of twinning and slip in cyclic deformation of extruded Mg-3%Al-1%Zn alloys, Scr. Mater. 63 (2010) 1077–1080.
[5] J.B. Jordon, J.B. Gibson, M.F. Horstemeyer, H.E. Kadiri, J.C. Baird, A.A. Luo, Effect of twinning, slip, and inclusions on the fatigue anisotropy of extrusion-textured AZ61 magnesium alloy, Mater. Sci. Eng. A 528 (2010) 6860–6871.
[6] L. Wu, S.R. Agnew, Y. Ren, D.W. Brown, B. Clausen, G.M. Stoica, H.R. Wenk, P. K. Liaw, The effects of texture and tension twinning on the low-cycle fatigue behavior of a rolled magnesium alloy, AZ31B, Mater. Sci. Eng. A 527 (2010) 7057–7067.
[7] S. Hong, S.H. Park, Y.H. Hun, C.S. Lee, Anisotropic fatigue behavior of rolled Mg–3Al–1Zn alloy, J. Mater. Res. 25 (2010) 966–971.
[8] S.H. Park, S.G. Hong, W. Bang, C.S. Lee, Effect of anisotropy on the low-cycle fatigue behavior of rolled AZ31 magnesium alloy, Mater. Sci. Eng. A 527 (2010) 417–423.
[9] S.H. Park, S.G. Hong, J. Yoon, C.S. Lee, Influence of loading direction on the anisotropic fatigue properties of rolled magnesium alloy, Int J. Fatigue 87 (2016) 201–215.
[10] S.H. Park, S.G. Hong, C.S. Lee, Role of initial {10–12} twin in the fatigue behavior of rolled Mg–3Al–1Zn alloy, Scr. Mater. 62 (2010) 666–669.
[11] A.N. Chamos, S.G. Pantelakis, G.N. Haidemenopoulos, E. Kamoutsi, Tensile and fatigue behavior of wrought magnesium alloys AZ31 and AZ61, Fatigue Fract. Eng. Mater. Struct. 31 (2008) 812–821.
[12] F. Lv, F. Yang, Q.Q. Duan, T.J. Luo, Y.S. Yang, S.X. Li, Z.F. Zhang, Tensile and low-cycle fatigue properties of Mg–2.8% Al–1.1% Zn–0.4% Mn alloy along the transverse and rolling directions, Scr. Mater. 61 (2009) 887–890.
[13] F. Lv, F. Yang, Q.Q. Duan, Y.S. Yang, S.D. Wu, S.X. Li, Z.F. Zhang, Fatigue properties of rolled magnesium alloy (AZ31) sheet: Influence of specimen orientation, Int. J. Fatigue 33 (2011) 672–682.
[14] S. Ishihara, S. Taneguchi, H. Shibata, T. Goshima, A. Saiki, Anisotropy of the fatigue behavior of extruded and rolled magnesium alloys, Int. J. Fatigue 50 (2013) 94–100.
[15] H. Zhang, D.X. Dong, S.J. Ma, C.F. Gu, S. Chen, X.P. Zhang, Effects of percent reduction and specimen orientation on the ratcheting behavior of hot-rolled AZ31B magnesium alloy, Mater. Sci. Eng. A 575 (2013) 223–230.
[16] S.G. Hong, S.H. Park, C.S. Lee, Role of {10–12} twinning characteristics in the deformation behavior of a polycrystalline magnesium alloy, Acta Mater. 58 (2010) 5873–5885.
[17] L. Wu, A. Jain, D.W. Brown, G.M. Stoica, S.R. Agnew, B. Clausen, Twinning–detwinning behavior during the strain-controlled low-cycle fatigue testing of a wrought magnesium alloy, ZK60A, Acta Mater. 56 (2008) 688–695.
[18] J. Koike, R. Ohyama, Geometrical criterion for the activation of prismatic slip in AZ61Mg alloy sheets deformed at room temperature, Acta Mater. 53 (2005) 1963–1972.
[19] S.R. Agnew, O. Duygulu, Plastic anisotropy and the role of non-basal slip in magnesium alloy AZ31B, Int. J. Plast. 21 (2005) 1161–1193.
[20] Q. Yu, J. Zhang, Y. Jiang, Q. Li, An experimental study on cyclic deformation and fatigue of extruded ZK60 magnesium alloy, Int. J. Fatigue 36 (2012) 47–58.
[21] Q. Yu, J. Zhang, Y. Jiang, Direct observation of twinning–detwinning–retwinning on magnesium single crystal subjected to strain-controlled cyclic tension–compression in [0001] direction, Philos. Mag. Lett. 91 (2011) 757–765.
[22] S.M. Yin, F. Yang, X.M. Yang, S.D. Wu, S.X. Li, G.Y. Li, The role of twinning–detwinning on fatigue fracture morphology of Mg–3%Al–1%Zn alloy, Mater. Sci. Eng. A 494 (2008) 397–400.
[23] D.W. Brown, A. Jain, S.R. Agnew, B. Clausen, Twinning and detwinning during cyclic deformation of Mg alloy AZ31B, Mater. Sci. Forum 539–543 (2007) 3407–3413.
[24] L. Wu, S.R. Agnew, D.W. Brown, G.M. Stoica, B. Clausen, A. Jain, D.E. Fielden, P. K. Liaw, Internal stress relaxation and load redistribution during the twinning–detwinning–dominated cyclic deformation of a wrought magnesium alloy ZK60A, Acta Mater. 56 (2008) 3699–3707.
[25] Y. Xiong, Q. Yu, Y. Jiang, An experimental study of cyclic plastic deformation of extruded ZK60 Magnesium alloy, J. Plast. 53 (2014) 107–124.
[26] Y. Xiong, Y. Jiang, An experimental study of cyclic plastic deformation of extruded ZK60 Magnesium alloy, Int. J. Fatigue 64 (2014) 74–83.
[27] C. Laird, Fatigue crack propagation, ASTM STP 415 (1967) 131–168.
[28] R.C. Zeng, E.H. Han, W. Ke, W. Dietzel, K.U. Kainer, A. Andrejs, Influence of microstructure on tensile properties and fatigue crack growth in extruded magnesium alloy AM60, Int. J. Fatigue 32 (2010) 411–419.
[29] R.C. Zeng, Y.B. Xu, E.H. Han, W. Ke, Fatigue crack propagation behavior of as extruded magnesium alloy AZ80, Mater. Sci. Eng. A 509 (2009) 1–7.
[30] T.S. Shih, W.S. Liu, Y.J. Chen, Fatigue of as-extruded AZ61A magnesium alloy, Mater. Sci. Eng. A 325 (2002) 152–162.
[31] J.D. Morrow, Internal friction, damping, and cyclic plasticity, ASTM STP 378 (1965) 45–87.
[32] S.H. Park, S. Hong, B.H. Lee, W. Bang, C.S. Lee, Low-cycle fatigue characteristics of rolled Mg-3Al-1Zn alloy, Int. J. Fatigue 32 (2010) 1835–1842.